Available online at www.sciencedirect.com
ScienceDirect
Inorganica Chimica Acta 361 (2008) 947–955
Inorganica Chimica Acta
www.elsevier.com/locate/ica

Spectroscopic characterization of a Ni-organic radical intermediate in the aerobic oxidation of methanol catalyzed by a Ni(II)(polyoximate) complex

Sara E. Edison [a], Sean D. Conklin [a], Necati Kaval [a], Lionel E. Cheruzel [b], Jeanette A. Krause [a], Carl J. Seliskar [a], William R. Heineman [a], Robert M. Buchanan [b], Michael J. Baldwin [a,*]

[a] *Department of Chemistry, University of Cincinnati, Cincinnati, OH 45221, United States*
[b] *Department of Chemistry, University of Louisville, Louisville, KY 40292, United States*

Received 27 April 2007; accepted 15 May 2007
Available online 26 May 2007

Dedicated to Edward Solomon.

Abstract

In the aerobic oxidation of methanol catalyzed by a Ni(II)(TRISOX) complex [H_3TRISOX = tris(1-propan-2-onyl oxime)amine], an intermediate is observed spectroscopically. The intensities of both the UV–Vis absorption and electron paramagnetic resonance (EPR) spectra associated with this intermediate maximize during the time period of maximum formaldehyde production, and decrease as the methanol oxidation activity decreases. The UV–Vis spectrum has prominent features at 350, 420, and 535 nm. The EPR spectrum is centered at $g = 2.00$ and shows splittings of 28 ± 5 G. Both of these spectra are consistent with characterization of the intermediate as including one or more iminoxyl radicals derived from the oximate groups of the TRISOX ligand. Spectroscopic features very similar to those in the air-oxidized intermediate are observed in electrochemically oxidized samples, suggesting that the electrochemically generated complex will be a useful model for the intermediate observed during catalytic turnover. The crystal structure of a Ni(II) complex with an intermediate protonation state of the ligand, $[Ni(II)_2(H_2TRISOX)_2(\mu_2{:}\eta^1\text{-}ONO_2)](NO_3) \cdot (CH_3CN) \cdot 5(H_2O)$, **4**, has been structurally characterized. Comparison to the previously reported $[Ni(II)(H_2TRISOX)(CH_3CN)]_2(ClO_4)_2$, **3**, shows that bis(μ-oximate) dimers can form either with or without an additional bridging ligand. Addition of the nitrato bridge decreases the Ni–Ni distance from 3.5752(13) Å in **3** to 3.2014(4) Å in **4**. It is intriguing to note that the reactions catalyzed by the Ni(II)(TRISOX) complex, the net transfer of two hydrogen atoms from an alcohol or amine substrate to O_2, are the same reactions catalyzed by several different metalloenzymes that also incorporate both a redox active metal and a redox active organic component in their active sites.

Keywords: Ni complexes; Oxime; Iminoxyl radical; EPR; Isotopic label; Aerobic oxidation

1. Introduction

Use of oxygen as the oxidant in organic substrate oxidations (aerobic oxidation) is desirable since it is inexpensive and readily available, and it is far more environmentally friendly than classical stoichiometric oxidants like dichromate and permanganate [1]. However, while substrate oxidation by O_2 is often favorable thermodynamically, typically these reactions are kinetically challenged. Thus, a catalyst is required to promote aerobic substrate oxidation. A common strategy in developing such catalysts has been to use biomimetic chemistry, modeling the active site of a metalloenzyme that catalyzes the desired chemistry. An alternative strategy that we have pursued is to develop

* Corresponding author.
E-mail address: michael.baldwin@uc.edu (M.J. Baldwin).

0020-1693/$ - see front matter © 2007 Elsevier B.V. All rights reserved.
doi:10.1016/j.ica.2007.05.025

a catalyst with a metal oxidation state that is not usually reactive with O_2, surmising that if the oxygen reactivity with that metal is unusual, so will be the substrate oxidations that it promotes. Our choice of metal oxidation state has been Ni(II), which is not generally considered oxygen active. While reaction of Ni(II) complexes with oxygen is not unprecedented [2–4], it is generally driven by *irreversible* ligand oxidation [4–6], and is thus not catalytically viable. The ligand donor groups that we have found useful in promoting the oxygen reactivity of Ni(II) complexes are oximates [7,8]. These were initially chosen due to their ability to form stable, low potential Ni(III) and Ni(IV) complexes [9–14].

Nickel(II) and the ligand H_3TRISOX (tris(1-propan-2-onyl oxime)amine), a tetradentate, tripodal amine with three oxime-containing arms [15], form a complex that reacts with oxygen in the presence of a suitable substrate when the oximes of $[Ni(II)(H_3TRISOX)(NO_3)(H_2O)](NO_3)$, **1**, are deprotonated by the addition of three equivalents of base per Ni(TRISOX) unit [7,8]. The oximate-bridged dimer structure that has been structurally characterized for an intermediate protonation state suggests that the oxygen-active Ni(TRISOX) complex, **2**, is also a dimer [7]. This complex promotes multiple turnovers of aerobic oxidation of primary alcohol or amine substrates to the corresponding aldehyde or imine [8]. Among these substrates is methanol, for which very few examples of homogeneous, catalytic, aerobic oxidation to formaldehyde have been reported [16]. Additionally, this complex is an efficient catalase mimic, rapidly disproportionating a large excess of hydrogen peroxide [8].

The net reaction that is catalyzed by the Ni(TRISOX) complex is the transfer of two hydrogen atoms from the substrate to O_2 to form the substrate oxidation product (aldehyde or imine) and H_2O_2, as shown in Eq. (1) [8]:

$$RH_2 + O_2 \rightarrow R + H_2O_2 \quad (1)$$

The hydrogen peroxide is rapidly disproportionated by the catalase-like activity of Ni(TRISOX), leading to a 2:1 ratio of oxidation product to O_2 uptake. This reaction is thermodynamically favorable for all of the observed substrates, although there is a structural criterion for selectivity as well. Branching at the α-carbon prevents the reaction from taking place, leading to selective oxidation of only primary alcohols and certain amine substrates [8]. The reactions that are catalyzed by the Ni(II)(TRISOX) complex are the same reactions that are catalyzed in biology by the copper-containing enzymes, galactose oxidase (primary alcohol substrates) and amine oxidases (amine substrates) [17]. Both of these types of enzymes incorporate a redox-active metal, copper, and a redox active organic component, a modified tyrosyl in galactose oxidase [18,19] and a quinone cofactor in the amine oxidases [20], in their active sites. Similarly, the cholesterol oxidase activity of the Cu-containing β-amyloid protein associated with Alzheimer's disease [21], which occurs with the same net reaction as in Eq. (1), is proposed to involve hydrogen atom transfer mediated by a redox-active tyrosine residue [22].

In this paper, we describe the characterization of a spectroscopically observable intermediate in the aerobic oxidation of methanol promoted by the Ni(II)(TRISOX) complex. This intermediate builds up and then disappears on the same time scale as the observed uptake of oxygen and production of formaldehyde. A combination of several complementary spectroscopic and electrochemical methods identifies this intermediate as including an iminoxyl radical derived from the oximate groups of the ligand. Thus, this catalyst is analogous to galactose oxidase and the Cu-dependent amine oxidases not only by its reactivity, but by its characterization as a metal-organic redox hybrid catalyst as well.

2. Experimental

All materials were obtained from either Acros or Aldrich and used without further purification unless otherwise indicated, except for ^{15}N-labelled reagents, which were obtained from Cambridge Isotope Laboratories. The synthesis of $[Ni(II)(H_3TRISOX)(NO_3)(H_2O)](NO_3) \cdot H_2O$, **1**, has been reported previously [7]. This complex with the H_3TRISOX ligand labeled with ^{15}N in the distinct nitrogen positions was synthesized as reported for ^{15}N-labeled $Ni(H_3TRISOX)Cl_2$ [23]. Isotopically labeled complexes were crystallized and the unit cells were determined by X-ray crystallography to confirm that they were identical to those previously found for **1**.

UV/Vis absorption spectra of the aerobic reaction solution were collected using a Spectral Instruments Inc. 400 Series dip probe CCD-array spectrophotometer. A 1.0 mM sample of **1** was prepared by dissolving 13 mg (0.03 mmol) of the purple solid in 30 mL of methanol. The reaction was initiated by adding 0.1 mL of a methanolic 1.0 M tetrabutylammonium hydroxide solution in the presence of air or O_2, and spectra were repetitively obtained throughout the time-course of the reaction.

Spectroelectrochemical experiments were conducted on samples of **2**, in methanol or acetonitrile, generated by adding 3 equiv. of KOH to 1.0 mM solutions of **1**. The methanol experiments were conducted under anaerobic conditions in a transparent, Ar-purged box. The sample was electrochemically oxidized in an optically transparent thin layer electrode (OTTLE) cell consisting of indium–tin oxide (ITO) plates as the working electrode, a Ag/AgCl reference electrode and a platinum wire auxiliary electrode. Sodium perchlorate was the supporting electrolyte and a Hewlett–Packard Model 8453 spectrometer was used to collect the UV/Vis absorption spectrum as a potential was applied.

Electron paramagnetic resonance (EPR) spectra were recorded on a Varian Associates E-109 spectrometer. The magnetic field was calibrated using a Varian E-500 NMR Gauss meter. Microwave frequencies were between 9.45 and 9.49 GHz with a microwave power of 20 mW. An

insert dewar was used to keep the samples at liquid nitrogen temperature. Air-oxidized samples were prepared from 30 mM **1** in methanol. KOH was added to initiate the reaction, which was quenched by freezing in liquid nitrogen at various time points. Electrochemically oxidized samples were prepared from 5 mM **1** and methanolic KOH under Ar at −40 °C with a bulk electrolysis cell purchased from Bioanalytical Systems, Inc. and a BAS 50 W electrochemical analyzer. The supporting electrolyte was 100 mM $NaClO_4$.

2.1. X-ray crystallography of $[Ni(II)_2(TRISOXH_2)_2(\mu_2{:}\eta^1\text{-}ONO_2)](NO_3)\cdot(CH_3CN)\cdot 5(H_2O)$, **4**

Single crystals of **4** were obtained by dissolving approximately 8 mM of **1** in wet CH_3CN. This was allowed to sit with excess, solid KOH for about 10 min, filtered, and set up for vapor diffusion of ethyl acetate into the solution under argon. For X-ray examination and data collection, a suitable purple plate-like crystal was mounted in a Cryo-loop with paratone-N. Diffraction data were collected at 150 K on a SMART6000 CCD diffractometer with graphite-monochromated Mo Kα radiation, $\lambda = 0.71073$ Å. The data frames were processed using SAINT. The data were corrected for decay, Lorentz and polarization effects. Absorption and beam corrections based on the multi-scan technique were applied using SADABS. The structure was solved by a combination of the Patterson method and the difference Fourier technique using SHELXTL [24]. The model was refined by full-matrix least squares on F^2. The oxime H-atoms were located directly and the positions refined. The water H-atoms were located directly and were held fixed at that location. The remaining H-atoms were either located directly or calculated. A riding model was applied for all H-atoms with the exception of the oximes. All non-hydrogen atoms were refined with anisotropic displacement parameters. The hydrogen atom

Table 1
Crystal data and structure refinement for **4**

Formula	$C_{18}H_{34}N_9O_9Ni_2\cdot CH_3CN\cdot 5H_2O$
Formula weight	769.10
Temperature (K)	150(2)
Wavelength (Å)	0.71073
Crystal system/space group	triclinic/$P\bar{1}$
Unit cell dimensions	
a (Å)	9.6150(10)
b (Å)	10.5920(11)
c (Å)	17.0107(18)
α (°)	98.597(2)
β (°)	100.828(2)
γ (°)	103.751(2)
Volume (Å^3), Z	1618.2(3), 2
Absorption coefficient (mm^{-1})	1.242
$F(000)$	810
Crystal size (mm)	$0.31\times0.20\times0.08$
θ Range for data collection (°)	2.02–28.32
Limiting indices	$-12\leqslant h\leqslant 12$, $-14\leqslant k\leqslant 14$, $-22\leqslant l\leqslant 22$
Reflections collected	22135
Data/R_{int}/restraints/parameters	8017/0.0304/0/436
Absorption correction, maximum/minimum transmission	multi-scan, 0.9072/0.6994
Goodness-of-fit on F^2	1.049
R_1/wR_2 $[I>2\sigma(I)]$	0.0317/0.0843
R_1/wR_2 (all data)	0.0375/0.0882

Table 2
Selected bond lengths (Å) and angles (°) for **4**

Ni(1)–N(2)	2.0161(15)	Ni(1)–O(8)	2.0407(12)
Ni(1)–N(1)	2.0724(15)	Ni(1)–N(3)	2.0782(16)
Ni(1)–N(4)	2.1197(16)	Ni(1)–O(7)	2.1675(13)
Ni(2)–N(7)	2.0239(14)	Ni(2)–O(8)	2.0513(12)
Ni(2)–N(6)	2.0612(14)	Ni(2)–N(5)	2.0660(15)
Ni(2)–O(2)	2.1044(13)	Ni(2)–N(8)	2.1119(15)
O(1)–N(1)	1.404(2)	O(2)–N(2)	1.3666(18)
O(3)–N(3)	1.3851(19)	O(5)–N(5)	1.3973(19)
O(6)–N(6)	1.3969(19)	O(7)–N(7)	1.3792(18)
O(8)–N(9)	1.307(2)	O(9)–N(9)	1.260(2)
O(10)–N(9)	1.290(2)		
N(2)–Ni(1)–O(8)	90.15(5)	N(2)–Ni(1)–N(1)	159.79(6)
O(8)–Ni(1)–N(1)	108.27(6)	N(2)–Ni(1)–N(3)	92.44(6)
O(8)–Ni(1)–N(3)	99.71(6)	N(1)–Ni(1)–N(3)	92.53(6)
N(2)–Ni(1)–N(4)	81.66(6)	O(8)–Ni(1)–N(4)	171.74(6)
N(1)–Ni(1)–N(4)	79.99(6)	N(3)–Ni(1)–N(4)	79.62(6)
N(2)–Ni(1)–O(7)	85.40(5)	O(8)–Ni(1)–O(7)	87.87(5)
N(1)–Ni(1)–O(7)	87.02(5)	N(3)–Ni(1)–O(7)	172.13(6)
N(4)–Ni(1)–O(7)	92.57(5)	N(7)–Ni(2)–O(8)	90.93(5)
N(7)–Ni(2)–N(6)	159.75(6)	O(8)–Ni(2)–N(6)	108.47(5)
N(7)–Ni(2)–N(5)	97.23(6)	O(8)–Ni(2)–N(5)	97.07(5)
N(6)–Ni(2)–N(5)	86.36(6)	N(7)–Ni(2)–O(2)	86.24(6)
O(8)–Ni(2)–O(2)	87.68(5)	N(6)–Ni(2)–O(2)	88.73(6)
N(5)–Ni(2)–O(2)	174.05(5)	N(7)–Ni(2)–N(8)	80.85(6)
O(8)–Ni(2)–N(8)	171.03(5)	N(6)–Ni(2)–N(8)	80.10(6)
N(5)–Ni(2)–N(8)	80.55(6)	O(2)–Ni(2)–N(8)	95.30(5)
N(9)–O(8)–Ni(1)	131.94(11)	N(9)–O(8)–Ni(2)	121.86(11)
Ni(1)–O(8)–Ni(2)	102.96(5)	C(5)–N(2)–O(2)	120.54(15)
C(5)–N(2)–Ni(1)	116.64(12)	O(2)–N(2)–Ni(1)	121.77(11)
C(17)–N(7)–O(7)	120.27(14)	O(7)–N(7)–Ni(2)	121.89(11)

Table 3
Hydrogen bonds (Å and °) for **4**

D–H···A	d(D–H)	d(H···A)	d(D···A)	∠(DHA)
O1–H1···O33[a]	0.88(3)	1.92(3)	2.730(2)	153(3)
O(3)–H(3)···O9[b]	0.86(3)	1.65(3)	2.512(2)	175(3)
O(5)–H(5)···O10[b]	0.84(3)	1.80(3)	2.631(2)	168(3)
O(6)–H(6)···O10[b]	0.88(3)	1.81(3)	2.681(2)	169(3)
O30–H30A···O34B[b]	0.88	1.99	2.835(4)	161
O30–H30A···O34A[b]	0.88	2.13	2.975(7)	161
O30–H30B···O33[c]	0.72	2.15	2.869(2)	177
O31–H31A···O2[b]	0.90	1.83	2.730(2)	174
O31–H31B···O31[d]	0.94	1.94	2.871(4)	171
O32–H32A···O7[b]	0.89	2.03	2.906(2)	168
O32–H32B···O6[a]	0.91	1.86	2.765(2)	173
O33–H33A···O32[b]	0.85	1.98	2.770(2)	156
O33–H33B···O30[a]	0.89	1.99	2.853(2)	163
O34B–H34A···N20[b]	0.87	2.36	3.134(5)	149
O34B–H34B···O10[b]	0.79	1.97	2.713(3)	158

Symmetry operators: [a] $-x+1$, $-y+1$, $-z+1$; [b] x, y, z; [c] $x+1$, $y+1$, z; [d] $-x$, $-y+1$, $-z$.

isotropic temperature factors were defined as $a * U_{eq}$ of the adjacent atom ($a = 1.5$ for –OH and CH_3 and 1.2 for all others). Water molecule, O34, is disordered, occupancy set at 0.65:0.35 for the two components. Crystal and refinement data are summarized in Table 1. Selected bond distance and angle information are collected in Table 2. Hydrogen bonding information is given in Table 3.

3. Results

3.1. Overview of reaction course

Addition of base to air saturated solutions of **1** in methanol at room temperature results in immediate uptake of O_2 and production of formaldehyde. Although this reactivity continues for several hours, it is most efficient during the first few minutes and has tapered off substantially within tens of minutes [8]. Once most of the H-atom transfer reactivity (methanol oxidation) has ended, after 1–2 h, oxidation of about 2 equiv. of triphenylphosphine to triphenylphosphine oxide, which is not produced earlier in the catalyst lifetime, is observed [25]. Incorporation of ^{18}O from $^{18}O_2$ into the Ph_3PO product previously demonstrated that this is the result of oxygen atom transfer to Ph_3P from an O_2-derived species rather than oxidation of Ph_3P followed by nucleophilic attack by water [7]. Thus, as the H-atom transfer reactivity is diminished by degradation of the catalyst, the altered Ni(TRISOX)-derived complex exhibits O-atom transfer reactivity until the oxygen reactivity is exhausted. The species that builds up during the 1–3 h time period with O-atom transfer ability is associated with a classical Ni(III) EPR spectrum that we reported previously [7]. An intermediate that is observable by UV/Vis and EPR spectroscopies is associated with the initial methanol oxidation activity, with spectroscopic features whose appearance and decay coincide with this H-atom transfer activity under turnover conditions.

3.2. UV–Vis spectra

Addition of base to an anaerobic methanol solution of **1** results in a change in the shade of purple of the solution. Exposure of that solution to air results in a color change to brown. Similarly, addition of base to an oxygen- or air-saturated solution of **1** results in a rapid change from purple to brown. This change was followed over time at room temperature using a UV/Vis spectrophotometer coupled to a fiber optic dip probe. These data are shown in Fig. 1. The overall intensity increases during the first 40–90 s, followed by a much slower loss in intensity over the next hour. The absorption features at 350, 420, and 535 nm grow in on a similar time scale; however, significant intensity remains in the region of the 535 nm feature once the higher energy features have disappeared.

UV/Vis spectra of electrochemically oxidized solutions of **2** were obtained using an OTTLE cell. The spectrum

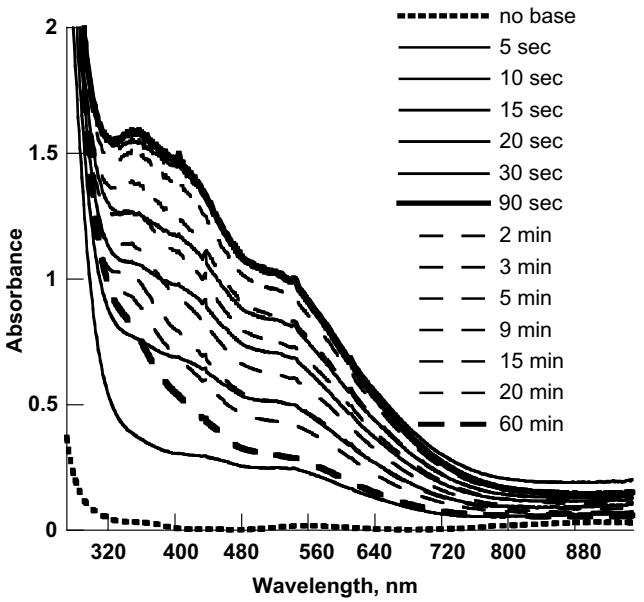

Fig. 1. UV–Vis spectra of the room-temperature aerobic reaction of **2** in methanol at selected time points, initiated by addition of base. Solid lines indicate time points with increasing absorption intensity, and dashed lines indicate time points at which the intensity is decreasing. The spectrum with the short dashes is of the sample immediately prior to base addition.

obtained in acetonitrile is generally similar to the air-oxidized intermediate, with the most intense absorption band at 360 nm and an intense shoulder at about 500 nm. The spectrum obtained in methanol under anaerobic conditions is nearly identical to that of the air-oxidized intermediate, as shown in Fig. 2.

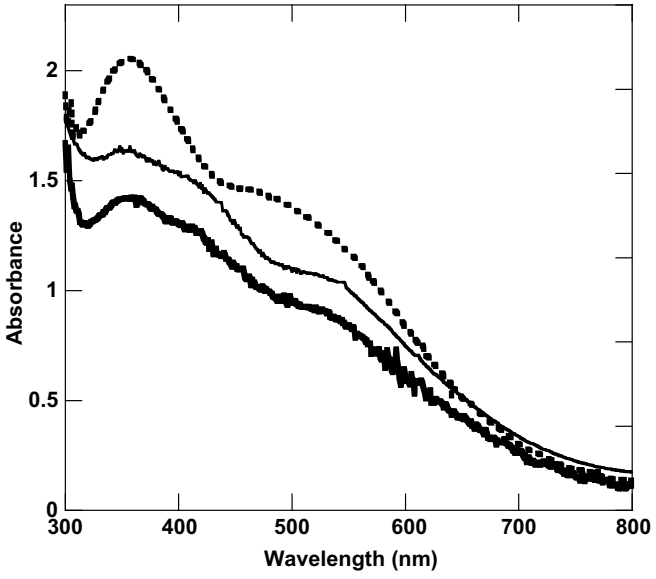

Fig. 2. UV–Vis spectra of oxidized solutions of **2**. The bold lines are electrochemically oxidized using an OTTLE cell in methanol (solid) or acetonitrile (dashed). The fine solid line is the air-oxidized spectrum in methanol as in Fig. 1, for comparison.

3.3. EPR spectra

EPR spectra of samples that were freeze-quenched in liquid nitrogen at a series of time points throughout the reaction of **2** with air and methanol show a feature centered at $g = 2.00$ that evolves and disappears along with the UV/Vis spectrum and the methanol oxidation activity. The magnitude of the splittings within this feature is 28 ± 5 G. As this feature disappears over tens of minutes, it is replaced by the Ni(III) feature that was reported previously [7]. The EPR spectra at selected times are shown in Fig. 3. Isotopic labeling of the amine nitrogen in the TRISOX ligand with ^{15}N shows no significant change in the $g = 2.00$ signal, although the nitrogen superhyperfine on $g_{\perp}$ of the Ni(III) feature that grows in later collapses from three lines to two. In contrast, ^{15}N labeling of the oxime nitrogens has little effect on the Ni(III) signal, but has a dramatic effect on the $g = 2.00$ feature. The EPR spectra of the nitrogen isotopomers of **2** exposed to air in methanol are shown in Fig. 4.

Complex **2** was electrochemically oxidized by anaerobic bulk electrolysis at -40 °C in either acetonitrile or methanol. The EPR spectrum of the complex oxidized in acetonitrile is very similar to the $g = 2.00$ EPR spectrum of the air-oxidized intermediate in methanol, as shown in Fig. 5. EPR spectra of the complex electrochemically oxidized in methanol show no EPR signals in the $g = 2$ region.

3.4. X-ray crystal structure of $[Ni(II)_2(TRISOXH_2)_2(\mu_2{:}\eta^1\text{-}ONO_2)](NO_3)\cdot(CH_3CN)\cdot 5(H_2O)$, **4**

Although the "fully deprotonated", oxygen-active complex **2** has so far defied attempts at its crystallization, the crystal structure of a complex in an intermediate protonation state, $[Ni(II)(H_2TRISOX)(CH_3CN)]_2(ClO_4)_2$, **3**, has been reported [7]. In that complex, one oxime from each Ni(TRISOX) unit is deprotonated and forms a μ(N–O) oximate bridge to a second Ni(II). The counter ion is the poorly coordinating perchlorate, so no additional bridges

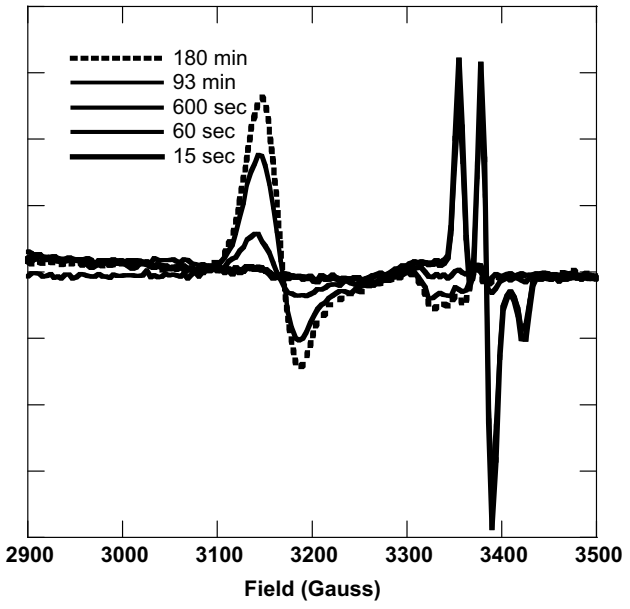

Fig. 3. EPR spectra of the room-temperature aerobic reaction of **2** in methanol at selected time points, initiated by addition of base. Reactions were quenched in liquid nitrogen, and spectra were collected at that temperature.

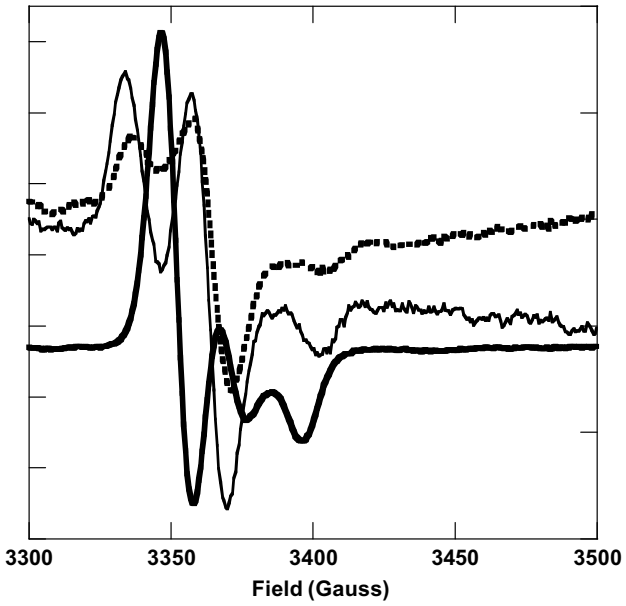

Fig. 4. EPR spectra of the room-temperature aerobic reaction of **2** in methanol quenched about 40 s after initiation of the reaction by cooling in liquid nitrogen. The fine solid line is the spectrum of the natural abundance complex, the bold solid line is of the complex with the oxime nitrogens ^{15}N-labelled, and the dashed line is the spectrum with the amine nitrogen ^{15}N-labelled.

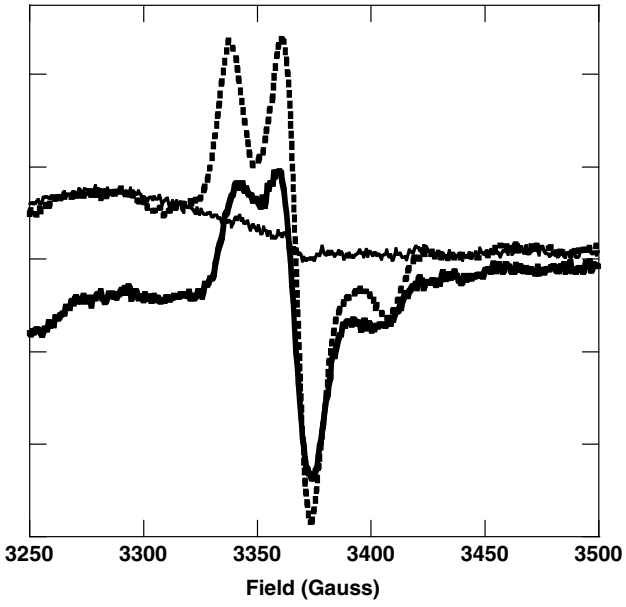

Fig. 5. EPR spectra of **2** after electrochemical oxidation in acetonitrile (bold solid) or methanol (fine solid). The dashed line is the air-oxidized sample as in Figs. 3 and 4, for comparison.

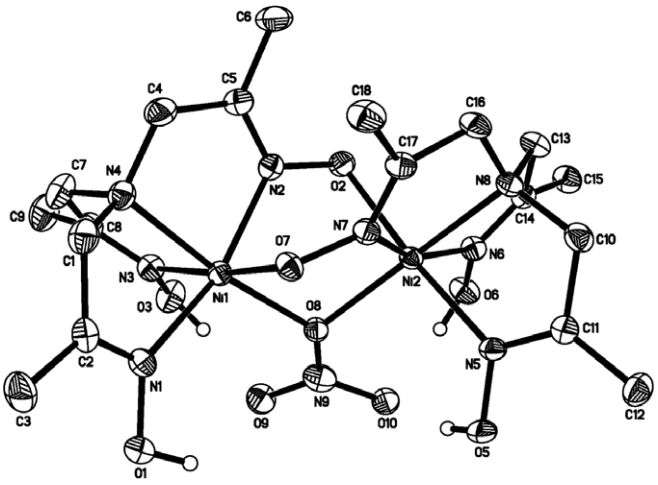

Fig. 6. ORTEP diagram of **4**. Hydrogen atoms, except for oxime hydrogens on O(1), O(3), O(5), and O(6), are omitted for clarity, as are the non-coordinated nitrate counter ion and solvents of crystallization. (50% probability thermal elliposoids).

are present. Since an additional bridge may be present in the oxygen-active complex **2**, or in an intermediate in the catalytic cycle, a complex in the same intermediate protonation state as **3**, but with a potentially bridging anion, nitrate, was structurally characterized. In this complex, crystallized as $[Ni(II)_2(H_2TRISOX)_2(\mu_2{:}\eta^1\text{-}ONO_2)](NO_3)\cdot(CH_3CN)(H_2O)_5$, **4**, the two oximate groups form bridges between the two Ni(II) ions as in the previously reported dimer, but an additional nitrate bridge is present as well. The structure of **4** is shown in Fig. 6. The nitrate forms a single-atom bridge between the two nickels through an oxygen atom, reducing the Ni–Ni distance from 3.5752(13) Å in **3** to 3.2014(4) Å in **4**. Three of the four oxime protons (on O(3), O(5), and O(6)) form relatively strong hydrogen bonds to the bridging nitrate. Similar intramolecular hydrogen bonding is observed in a number of $Ni(II)(H_3TRISOX)X_2$ complexes [26], where X is a coordinated anion or water, as well as Ni(II) complexes with derivatives of H_3TRISOX in which one of the three oxime groups is substituted by another functional group [27].

4. Discussion

The aerobic oxidation of methanol catalyzed by the Ni(II)(TRISOX) complex, **2**, to formaldehyde is an intriguing reaction system. It involves a multi-step reaction cycle that depends on the presence of substrate for any oxygen reactivity to be observed. It is further complicated by a change in reactivity from hydrogen atom transfer to oxygen atom transfer as the catalyst changes over the course of multiple turnovers and eventually loses its oxygen activity. This change in reactivity is accompanied by an EPR signal that is typical of Ni(III) with N/O coordination. There is some evidence for a different, albeit similar, Ni(III) EPR signal at the initial stages of the reaction under certain conditions [28], though the relationship between this EPR signal and substrate oxidation, and the conditions that result in its generation, have yet to be well defined. During the time period between observation of these two Ni(III) EPR signals, an intermediate is generated that clearly corresponds in its build-up and decay to the aerobic methanol oxidation activity of **2**. The UV/Vis absorption spectrum associated with this intermediate maximizes in intensity after about 60 s, and then decays over tens of minutes, in a manner that is consistently reproducible at room temperature. Furthermore, similar UV/Vis spectra are associated with methanol oxidation by Ni(II) complexes with derivatives of the TRISOX ligand, and in aerobic oxidation reactions of other substrates by **2** [25]. The data presented here allow characterization of this intermediate, which may have broader significance for aerobic substrate oxidation reactions that occur by net hydrogen atom transfer.

Time-dependent monitoring of the reaction shows UV/Vis absorption and EPR spectra that correspond in their change in intensity to the rate of formaldehyde production. Both of these spectroscopic signatures are consistent with data reported for iminoxyl radicals generated by oxidation of oximes. Everett and coworkers determined the UV–Vis spectrum of an oxime-derived iminoxyl radical [29]. It features a strong absorption at 350 nm, a shoulder at about 400 nm, and a less intense absorption at 620 nm. These are strikingly similar to the features observed in Figs. 1 and 2. Furthermore, the relatively large ^{14}N splittings of the $g = 2.00$ signal in the EPR spectrum are similar to those for other oxime-derived iminoxyl radicals, reported first by Thomas [30] and later by Ingold and coworkers [31,32], to be around 30 G in X-band. The EPR signal of the intermediate is broadened by interaction with the paramagnetic nickel so that the proton superhyperfine observed in the published spectra of iminoxyl radicals are not resolved here. The unpaired electron density in the intermediate that generates the EPR signal is shown to be primarily on the oxime nitrogens by the significant change in the EPR spectrum when the oxime nitrogens of the TRISOX ligand are substituted with ^{15}N. No change in this signal is observed upon isotopic substitution of the amine nitrogen. This confirms that in this intermediate state, the oxidation equivalents are localized on the oximates. Simulations of these spectra have so far not been satisfactory, so further interpretation of the EPR spectra at this time would be premature. The simulations appear to be complicated by the interaction of the iminoxyl radical with the nickel, the presence of multiple oxidizable oximates in the complex, and the possibility that the spectrum has contributions from more than one similar species [28].

The similarity between the UV/Vis and EPR spectra of the electrochemically oxidized species and the intermediate generated by the oxygen reaction confirm that this intermediate is indeed an oxidized version of the Ni(TRISOX) complex. In the UV/Vis spectroelectrochemistry experiment, in which a potential is constantly applied to a small sample volume keeping the species in its oxidized state, the spectrum obtained in methanol more closely resembles the

intermediate spectrum in the aerobic methanol oxidation experiment than does the spectrum obtained in acetonitrile. While the acetonitrile spectrum is similar and thus suggests a similar oxidized species, the greater similarity of the methanol spectrum indicates that solvent interactions are important in the appearance of this spectrum. Since methanol is a substrate and acetonitrile is not, this may indicate substrate binding to the nickel. Alternatively, the solvation interactions between the complex and a protic versus a non-protic solvent with different dielectric constants may also alter the spectrum. The electrochemically generated EPR samples were prepared by bulk electrolytic application of current over time. Generation in acetonitrile of an EPR spectrum that is very similar to that of the air-oxidized intermediate confirms that substrate is not necessary for oxidation of the oximates to iminoxyl radicals. In methanol on the other hand, no EPR signal is observed in the bulk electrolysis experiment. This is presumably due to reaction of the oxidized species with methanol as the electrolysis proceeds, preventing the EPR-active species from building up as it does in acetonitrile, which is not an oxidation substrate.

The data presented here provide initial characterization of the intermediate as featuring an iminoxyl radical derived from one or more oximate groups of the TRISOX ligand, likely coupled to Ni(II). Extending the EPR spectroscopy to additional frequencies will help sort out different contributions to the EPR spectrum [28], aiding in the simulations which will provide more specific information about the radicals and their interactions. The electrochemical experiments show that an electrochemically generated model of the intermediate will be useful as well. It will provide samples for EPR that will have a much larger fraction of the Ni complexes in the oxidized (intermediate-like) state than occurs in the genuine air-oxidized intermediate during the multi-step turnover. Our current estimate of the fraction of Ni complex in the iminoxyl intermediate state at its maximum concentration during turnover is 10–20%, based on comparison of the integrated EPR intensity to the electrochemically generated EPR signal, and to a $CuSO_4$ standard. The higher percentage of oxidized species generated electrochemically will also allow XANES experiments to definitively assign the oxidation state of nickel in the iminoxyl complex, without the current caveat that the fraction of Ni in this state may be too low during catalytic turnover to distinguish an oxidation state change. Furthermore, while resonance Raman experiments on the freeze-quenched intermediate have not produced useful spectra, the high concentration of oxidized complex produced by the OTTLE cell and the ability to convert back and forth between oxidized and reduced complexes is anticipated to provide substantially improved data from resonance Raman spectroelectrochemistry experiments. Previously published Raman spectra of complexes closely related to **1** have definitively identified 28 vibrational modes of the neutral H_3TRISOX ligand bound to Ni(II) [23]. Preliminary DFT calculations on different protonation and oxidation states of acetone oxime, as a model of the oxime groups of TRISOX, suggest that the Raman spectra will clearly distinguish different oxidation and protonation states of the ligand in the intermediate-like complex [33].

The requirement for the presence of substrate in order to observe any oxygen reaction suggests a mechanism in which a very small equilibrium of oxygen binding to **2** occurs. The concentration of oxygen-bound species is too small to observe; however, in the presence of substrate, this low concentration of oxygen-bound complex reacts to produce the observed intermediate. This intermediate builds up as the small oxygen binding equilibrium continues to produce the oxygen-bound species which is fed into the substrate oxidation cycle. Even a very small equilibrium can lead to product build-up if it is followed by a sufficiently large equilibrium in the reaction cycle that proceeds to an irreversible step, as demonstrated previously in redox-mediated bridge exchange reactions of "substitution-inert" Mn(IV) dimers [34]. The crystal structure of complex **4** demonstrates that the Ni(TRISOX) framework can accommodate at least one exogenous bridge, although to accommodate two exogenous bridges or a side-on peroxide, one or more oximates would have to dissociate from the Ni (either as the oxidized iminoxyl radical or the protonated neutral oxime). Such dissociation of an oxime arm of H_3TRISOX upon addition of a more favorable ligand is observed in the crystal structure of $Zn(H_3TRISOX)(OAc)_2$ [35]. Furthermore, association of substrate is required to advance the reaction beyond the putative weak oxygen binding equilibrium, and is consistent with the solvent dependence of the features in the spectroelectrochemically generated UV–Vis spectrum compared to the intermediate. The hypothetical reaction cycle in Fig. 7 takes these considerations into account, though there is not as yet direct evidence for any of the specific structures suggested and a number of the structural details are speculative. In this scheme, there are two structures indicated to include iminoxyl radicals. Structure **5** includes a bound peroxide. Thus, lack of an obvious peroxide-to-Ni(II) charge transfer (CT) transition in the UV–Vis spectrum of the intermediate weighs against assignment of **5** as the observed intermediate. For an end-on peroxide bridging structure, this feature would be expected around 465 nm, as reported by Riordan, Brunold and coworkers [36]. However, a side-on structure like **5** has not yet been reported. By analogy to copper-peroxide complexes, the most intense peroxide-to-metal CT transition would be expected to be at a higher energy in the side-on case than the end-on case [37,38], but would still likely be observed. Furthermore, the requirement for substrate in order to observe the intermediate suggests that some hydrogen atom transfer event has likely occurred to form the observed intermediate. This has not yet occurred in structure **5**. The other iminoxyl-containing species is found in the next step of the proposed mechanism. Intramolecular hydrogen atom transfer from the coordinated substrate in **5** is hypothesized to lead to

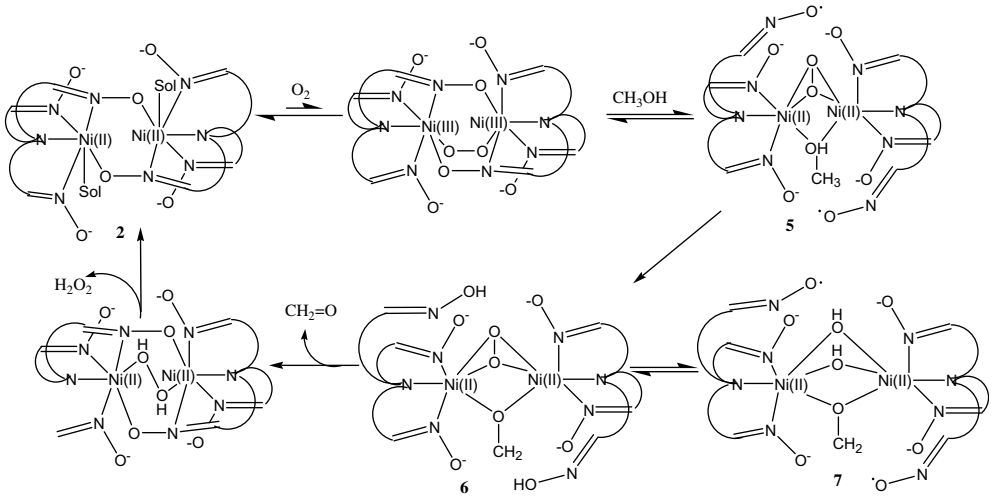

Fig. 7. Hypothetical reaction scheme for the aerobic oxidation of methanol catalyzed by **2**.

an equilibrium between two tautomers; in **6** the H-atoms occupy the iminoxyl radical positions from **5**, reducing them to neutral oximes, while in **7** the H-atoms reduce the peroxide to a pair of hydroxo groups. This is reminiscent of copper chemistry in which inter-conversion between a $Cu(II)_2$-peroxo species and a $Cu(III)_2$bis(oxo) species occurs [39,40]. Since **7** has no bound peroxide, the absence of a peroxide-to-nickel CT is not a concern. Furthermore, it is formed upon hydrogen atom transfer from substrate, in agreement with the observation that the H-atom donor substrate must be present for its observation. If this equilibrium lies toward **7**, then some accumulation of that species would be anticipated during turnover conditions, consistent with its assignment as the observed intermediate.

The number of examples of metalloenzymes such as those discussed in the introduction section that require both a metal ion (usually copper) *and* a redox active organic component for catalysis of net hydrogen atom transfer reactions suggests that the need for a redox-active ligand in the case reported here is not a coincidence. In fact, the only other transition metal complexes that have been shown to promote multiple turnovers of the aerobic oxidation of methanol to formaldehyde under homogeneous conditions also require a metal ion and a redox-active organic ligand [16]. Those complexes incorporate redox-active phenolate groups into the ligand, which are oxidized to phenoxyl radicals during catalytic turnover. Thus, it may be that there is some activation energy barrier to hydrogen atom transfer in these reactions that is more effectively overcome by involvement of an organic radical than by a transition metal radical alone. Indeed, iminoxyl radicals have been reported to abstract hydrogen atoms from a variety of substrates [32]. Better understanding of this Ni(TRISOX) system may help to elucidate that role of the redox-active organic component and its interaction with the metal ion in this type of biologically and commercially important aerobic oxidation.

Acknowledgement

Funding for this project was provided by the donors of the Petroleum Research Fund administered by the American Chemical Society (ACS-PRF 37653-AC3). Funding for the Smart6000 diffractometer was through NSF-MRI grant CHE-0215950. M.J.B. would also like to acknowledge Prof. Martin L. Kirk (University of New Mexico) for helpful discussions and Prof. James E. Penner-Hahn, Derek Yoder and Matthew Kidd (University of Michigan) for preliminary X-ray absorption spectroscopy experiments in support of this project and helpful discussions.

Appendix A. Supplementary material

CCDC 645276 contains the supplementary crystallographic data for **4**. These data can be obtained free of charge via http://www.ccdc.cam.ac.uk/conts/retrieving.html, or from the Cambridge Crystallographic Data Centre, 12 Union Road, Cambridge CB2 1EZ, UK; fax: (+44) 1223-336-033; or e-mail: deposit@ccdc.cam.ac.uk. Supplementary data associated with this article can be found, in the online version, at doi:10.1016/j.ica.2007.05. 025.

References

[1] R.A. Sheldon, in: B. Meunier (Ed.), Biocatalytic and Biomimetic Oxidations from an Industrial Perspective, Imperial College Press, London, 2000, 2000, p. 613.
[2] E.B. Paniago, D.C. Weatherburn, D.W. Margerum, Chem. Commun. (1971) 1427.
[3] E. Kimura, A. Sakonaka, R. Machida, J. Am. Chem. Soc. 104 (1982) 4255.
[4] C.A. Grapperhaus, M.Y. Darensbourg, Acc. Chem. Res. 31 (1998) 451.
[5] D. Chen, A.E. Martell, J. Am. Chem. Soc. 112 (1990) 9411.
[6] C.-C. Cheng, J. Gulia, S.E. Rokita, C.J. Burrows, J. Mol. Catal. A 113 (1996) 379.
[7] M.J. Goldcamp, S.E. Robison, J.A. Krause Bauer, M.J. Baldwin, Inorg. Chem. 41 (2002) 2307.

[8] S.E. Edison, R.P. Hotz, M.J. Baldwin, Chem. Commun. (2004) 1212.
[9] E.I. Baucom, R.S. Drago, J. Am. Chem. Soc. 93 (1971) 6469.
[10] A.N. Singh, R.P. Singh, J.G. Mohanty, A. Chakravorty, Inorg. Chem. 16 (1977) 2597.
[11] A.N. Singh, A. Chakravorty, Inorg. Chem. 19 (1980) 969.
[12] D.P. Martone, P. Osvath, A.G. Lappin, Inorg. Chem. 26 (1987) 3094.
[13] H.-J. Kruger, G. Peng, R.H. Holm, Inorg. Chem. 30 (1991) 734.
[14] S. Mandal, E.S. Gould, Inorg. Chem. 34 (1995) 3993.
[15] M.J. Goldcamp, J.A. Krause Bauer, M.J. Baldwin, Acta Cryst. E 58 (2002) o1354.
[16] P. Chaudhuri, M. Hess, J. Muller, K. Hildenbrand, E. Bill, T. Weyhermuller, K. Wieghardt, J. Am. Chem. Soc. 121 (1999) 9599.
[17] M.A. McGuirl, D.M. Dooley, Curr. Op. Chem. Biol. 3 (1999) 138.
[18] K. Clark, J.E. Penner-Hahn, M.M. Whittaker, J.W. Whittaker, J. Am. Chem. Soc. 112 (1990) 6433.
[19] K. Clark, J.E. Penner-Hahn, M. Whittaker, J.W. Whittaker, Biochemistry 33 (1994) 12553.
[20] S.M. Janes, M.M. Palcic, C.H. Scaman, A.J. Smith, D.E. Brown, D.M. Dooley, M. Mure, J.P. Klinman, Biochemistry 31 (1992) 12147.
[21] L. Puglielli, A.L. Friedlich, K.D.R. Setchell, S. Nagano, C. Opazo, R.A. Cherney, K.J. Barnham, J.D. Wade, S. Melov, D.M. Kovacs, A.I. Bush, J. Clin. Invest. 115 (2005) 2556.
[22] K.J. Barnham, F. Haeffner, G.D. Ciccotosto, C.C. Curtain, D. Tew, C. Mavros, K. Beyreuther, D. Carrington, C.L. Masters, R.A. Cherny, R. Cappai, A.I. Bush, FASEBJ 18 (2004) 1427.
[23] R.M. Jones, M.J. Baldwin, J. Phys. Chem. A 108 (2004) 3537.
[24] SMART v5.628 and SAINT v6.36A were used for data collection and processing. SADABS v2.10 was used for the application of the absorption and beam corrections. SHELXTL v6.12 was used for the structure solution. Neutral-atom scattering factors were used as stored in SHELXTL. G.M. Sheldrick, University of Göttingen, Germany and Bruker Analytical X-ray Solutions Inc., Madison, WI.
[25] S.E. Edison, Ph.D. Thesis, University of Cincinnati, Cincinnati, OH, 2004.
[26] R.M. Jones, M.J. Goldcamp, J.A. Krause, M.J. Baldwin, Polyhedron 25 (2006) 3145.
[27] M.J. Goldcamp, S.E. Edison, L.N. Squires, D.T. Rosa, N.K. Vowels, N.L. Coker, J.A. Krause Bauer, M.J. Baldwin, Inorg. Chem. 42 (2003) 717.
[28] S. Knottenbelt, M.L. Kirk, M.J. Baldwin, unpublished results.
[29] S.A. Everett, M.A. Naylor, M.R.L. Stratford, K.B. Patel, E. Ford, A. Mortenson, A.C. Furguson, B. Vojnovic, P. Wardman, J. Chem. Soc., Perkin Trans. 2 (2001) 1989.
[30] J.R. Thomas, J. Am. Chem. Soc. 86 (1964) 1446.
[31] J.L. Brokenshire, J.R. Roberts, K.U. Ingold, J. Am. Chem. Soc. 94 (1972) 7040.
[32] G.D. Mendenhall, K.U. Ingold, J. Am. Chem. Soc. 95 (1973) 2963.
[33] L. Prevette, R.M. Jones, M.J. Baldwin, unpublished results.
[34] M.J. Baldwin, N.A. Law, T.L. Stemmler, J.E. Penner-Hahn, V.L. Pecoraro, Inorg. Chem. 38 (1999) 4801.
[35] M.J. Goldcamp, J.A. Krause Bauer, M.J. Baldwin, J. Chem. Crystallogr. 35 (2005) 77.
[36] R. Schenker, M.T. Kieber-Emmons, C.G. Riordan, T.C. Brunold, Inorg. Chem. 44 (2005) 1752.
[37] M.J. Baldwin, P.K. Ross, J.E. Pate, Z. Tyeklar, K.D. Karlin, E.I. Solomon, J. Am. Chem. Soc. 113 (1991) 8671.
[38] M.J. Baldwin, D.E. Root, J.E. Pate, K. Fujisawa, N. Kitajima, E.I. Solomon, J. Am. Chem. Soc. 114 (1992) 10421.
[39] V. Mahadevan, M.J. Henson, E.I. Solomon, T.D.P. Stack, J. Am. Chem. Soc. 122 (2000) 10249.
[40] B.M.T. Lam, J.A. Halfen, V.G.J. Young, J.R. Hagadorn, P.L. Holland, A. Lledos, L. Cucurull-Sanchez, J.J. Novoa, S. Alvarez, W.B. Tolman, Inorg. Chem. 39 (2000) 4059.